Hindawi
Advances in Civil Engineering
Volume 2018, Article ID 3029837, 12 pages
https://doi.org/10.1155/2018/3029837

Research Article

A Designer's Approach for Estimation of Nuclear-Air-Blast-Induced Ground Motion

Shashank Pathak and G. V. Ramana

Department of Civil Engineering, Indian Institute of Technology Delhi, New Delhi, India

Correspondence should be addressed to Shashank Pathak; shashankpathaks@gmail.com

Received 19 August 2017; Accepted 5 December 2017; Published 8 March 2018

Academic Editor: Chiara Bedon

A reliable estimate of free-field ground displacement induced by nuclear-air-blast is required for design of underground strategic structures. A generalized pseudostatic formulation is proposed to estimate nuclear-air-blast-induced ground displacement that takes into account nonlinear stress-strain behaviour of geomaterials, stress-dependent wave propagation velocity, and stress wave attenuation. This proposed formulation is utilized to develop a closed-form solution for linearly decaying blast load applied on a layered ground medium with bilinear hysteretic behaviour. Parametric studies of closed-form solution indicated that selection of appropriate constrained modulus consistent with the overpressure is necessary for an accurate estimation of peak ground displacement. Stress wave attenuation affects the computed displacement under low overpressure, and stress-dependent wave velocity affects mainly the occurrence time of peak displacement and not its magnitude. Further, peak displacements are estimated using the proposed model as well as the UFC manual and compared against the field data of atmospheric nuclear test carried out at Nevada test site. It is found that the proposed model is in good agreement with field data, whereas the UFC manual significantly underestimates the peak ground displacements under higher overpressures.

1. Introduction

Underground siting of strategic structures [1] is an option to enhance the safety against nuclear-air-blast [2]. Nuclear explosions generate rapidly moving air-overpressures capable of producing significant ground displacements [3]. Most severe loading occurs within a close vicinity around the ground zero (GZ) known as superseismic zone. This zone is subjected to significantly high overpressures. The velocity of moving air-overpressure fronts is also more than the P-wave velocity of the ground [3–6]. Hence, a reliable estimate of nuclear-air-blast-induced ground displacement is required for design in superseismic zone [5, 7, 8]. Several studies using numerical approaches that account for realistic stress-strain behaviour and boundary conditions are reported for calculating the free-field response [9–16]. Such studies require specialized expertise in numerical tools and are unattractive to practicing engineers. Before the advent of computational tools, Wilson and Sibley [17] conceptualized a one-dimensional pseudostatic approach to estimate air-blast-induced ground displacement. Whitman [4] and Baron et al. [18] have also shown that air-blast-induced ground motion is predominantly one-dimensional and vertical in superseismic zone. In the present work, a generalized one-dimensional pseudostatic formulation is developed to estimate nuclear-air-blast-induced vertical ground displacement that accounts for (i) nonlinear stress-strain behaviour [e.g., 19, 20], (ii) stress-dependent wave propagation velocity, and (iii) stress wave attenuation. Using the proposed formulation, a closed-form solution is developed for linearly decaying blast load with negligible rise-time applied on a layered ground medium with bilinear hysteretic stress-strain behaviour. The proposed model is validated against the field data of an atmospheric nuclear test conducted at Nevada test site [21], and various parametric studies are carried out. In addition, performance of the closed-form solution is also compared with the model given in UFC [22].

2. Generalized Formulation

The developed formulation is explained in detail below.

2.1. Determination of Overstress Distribution (due to Air-Blast) in the Ground. Air-overpressure generated due to nuclear-air-blast consists of an initial rising portion followed by a decaying portion (Figure 1). Overpressure time-history can be visualized as consisting of multiple overpressure fronts. These overpressure fronts are transferred to the ground as P-waves. On arrival of an air-shock front at the point of interest, an initial pulse travels with seismic P-wave velocity and reaches a depth Z_{0i} at time t_i. Subsequently, other fronts arrive and penetrate into the ground. If the location of peak overpressure front at time t_i is given as Z_{pi}, then, the ground above the depth Z_{pi} experiences compressive stresses lower than those caused by the peak overpressure front at that depth. Therefore, the depths above Z_{pi} are referred to as "unloading zone." However, the peak overpressure front is yet to reach at locations deeper than Z_{pi}, and therefore, the zone lying beneath the depth Z_{pi} is denoted as "loading zone" (Figure 1). It is noted that "unloading zone" corresponds to the "decay portion" of overpressure, whereas "loading zone" corresponds to the "rising portion." Therefore, at times earlier than the rise-time, there does not exist any unloading zone as overpressure fronts from the decay portion do not arrive before the end of rise-time.

To determine the stress distribution in the ground at time t_i, contribution from all stress fronts arrived before time t_i is considered. If the kth overpressure front arrives at the point of interest on ground surface at time t_k such that $t_k \le t_i$, then the kth overpressure front reaches at depth Z_{ki} at time t_i. Stress fronts propagating through ground are affected by attenuation (caused by hysteresis losses, viscosity of ground materials, and dispersion of energy in 3-dimensional space) and interference with reflected wave fronts (generated due to impedance variation with depth). In the present study, stress wave attenuation is taken into account through a geometrical attenuation parameter, whereas interference of incident and reflected stress waves is ignored. If the attenuation coefficient at depth Z_{ki} is given as $\alpha(Z_{ki})$, then the stress generated at depth Z_{ki} can be written as $\alpha(Z_{ki}) \times P(t_k)$, where $P(t_k)$ is the magnitude of the kth overpressure front. Depth of the penetration Z_{ki} depends upon wave propagation velocity of the stress front, which in turn depends upon the tangential modulus of the geomaterial at the stress level at the depth of interest. If wave velocity of the kth stress front is denoted as V_{kz} (a function of depth "z"), then (1) can be solved to obtain Z_{ki} as a function of t_i, t_k, and V_{kz} (2),

$$\int_0^{Z_{ki}} \frac{\mathrm{dz}}{V_{kz}} = t_i - t_k, \tag{1}$$

$$Z_{ki} = g(t_i - t_k, V_{kz}) = \varphi(t_k), \tag{2}$$

where g is the function obtained by solving (1). It is noted that for a given t_i, Z_{ki} is effectively a function (φ) of t_k only because V_{kz} is also a function of t_k. As soon as the air-blast slaps the ground surface, ground deforms elastically and an elastic wave is generated which propagates with seismic P-wave velocity. Upon subsequent arrival of higher overpressure fronts, inelastic waves propagate at velocities smaller than P-wave velocity. If the ratio of P-wave velocity to wave velocity corresponding to the kth overpressure front at depth "z" is denoted as $f_{kz} = (V_{pz}/V_{kz})$, then at initial stress levels f_{kz} is equal to one. With increasing stress level, V_{kz} decreases [17, 23]; hence, it is logical to assume that f_{kz} increases with increasing stress level and the maximum value is attained at a peak stress level corresponding to the peak overpressure front. Therefore, a simplest choice is to assume a linearly increasing f_{kz} in direct proportion to overpressure (3). Overpressure fronts from the decay portion propagate through the media which is already stressed in a nonlinear range due to passage of the peak overpressure front. Therefore, it is assumed that wave velocity of overpressure fronts in the decay portion is the same as the peak overpressure front, and hence f_{kz} is the same as f_{rz}:

$$f_{kz} = \begin{cases} (f_{rz} - 1)\dfrac{P(t_k)}{P_o} + 1 \approx (f_{rz} - 1)\dfrac{t_k}{t_r} + 1, & 0 \le t_k \le t_r : \text{rising portion} \\ f_{rz}, & t_r \le t_k \le t_p : \text{decay portion,} \end{cases} \tag{3}$$

where subscript "z" represents the depth coordinate. Using the average loading rate as P_o/t_r, $P(t_k)/P_o$ can be approximated as t_k/t_r (3). As wave propagation velocity through ground media is proportional to the square root of the tangential modulus [24], f_{rz} is given by the following equation:

$$f_{rz} = \sqrt{\frac{(\partial\sigma_z/\partial\varepsilon_z)|_{\sigma=0}}{(\partial\sigma_z/\partial\varepsilon_z)|_{\sigma_{rz}}}}, \tag{4}$$

where $(\partial\sigma_z/\partial\varepsilon_z)|_{\sigma=0}$ is the tangential modulus at initial stress level at depth "z" and $(\partial\sigma_z/\partial\varepsilon_z)|_{\sigma_{rz}}$ is the tangential modulus at peak stress level at depth "z."

It should be noted that the ground is in equilibrium under geostatic stresses and at rest before nuclear explosion and only the overstresses caused by nuclear-air-blast causes the ground displacement.

2.2. Determination of Strain Distribution in Ground. Strain distribution with depth (ε_{iz}) can be determined using stress distribution (σ_{iz}) and an appropriate stress-strain relationship [e.g., 25–27] as given in the following equation:

$$\varepsilon_{iZ} = \begin{cases} f_L(z, \sigma_{iz}) : \text{loading} \\ f_U(z, \sigma_{iz}) : \text{unloading,} \end{cases} \tag{5}$$

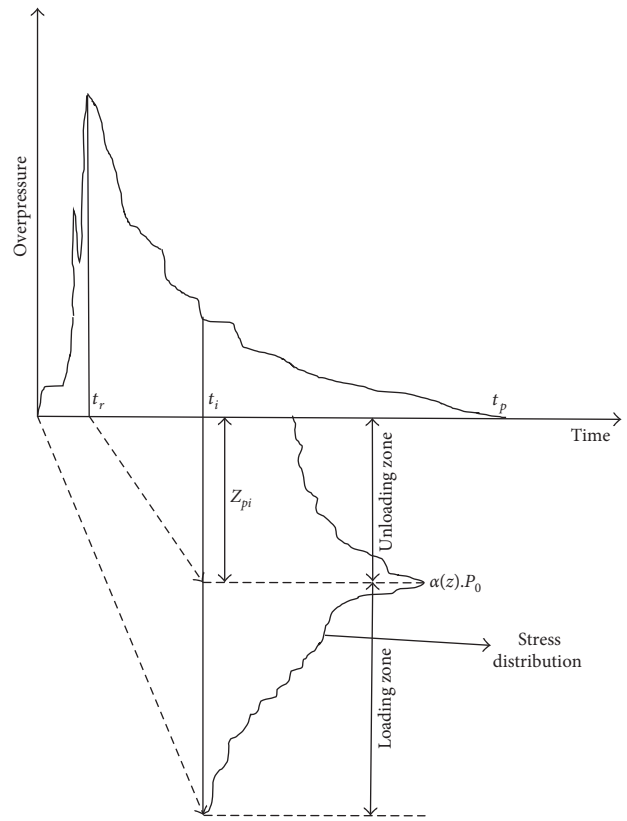

Figure 1: Schematic representation of dilatational stress distribution in ground at time t_i.

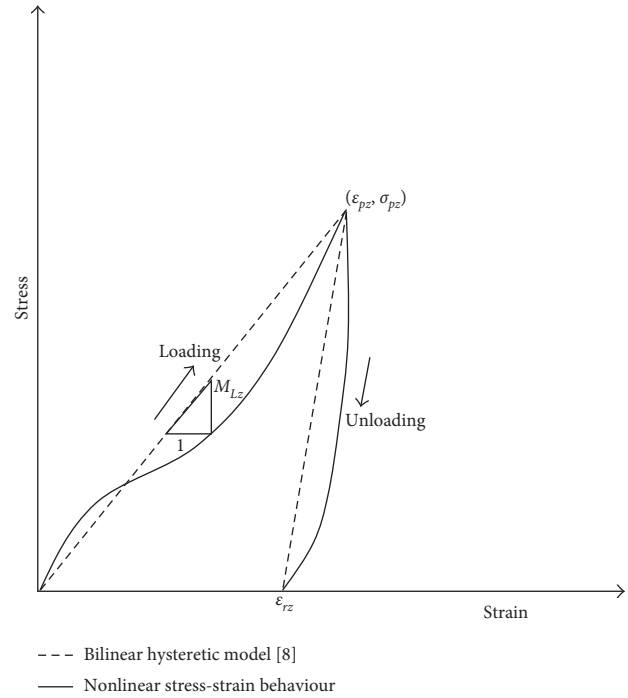

Figure 2: Schematic diagram for stress-strain relation at a depth "z."

where functions f_L and f_U denote the loading and unloading branches of the stress-strain curve, respectively (Figure 2).

2.3. Integration of Strains. To obtain the vertical ground displacement u_i at time instant t_i, the strain distribution is integrated (6) from the ground surface to the penetrated wavelength in the ground up to time $t_i\,(Z_{0i})$,

$$u_i = \int_0^{Z_{0i}} \varepsilon_{iz}\mathrm{d}z = \int_0^{Z_{ri}} f_U(z,\sigma)\mathrm{d}z + \int_{Z_{ri}}^{Z_{0i}} f_L(z,\sigma)\mathrm{d}z. \quad (6)$$

Substituting $Z = \varphi(t_k)$ in (6) leads to the following equation:

$$u_i = \begin{cases} \displaystyle\int_{t_i}^{0} f_L\Big(\varphi(t_k), \sigma\Big(\varphi(t_k)\Big)\Big) \times \varphi'(t_k)\mathrm{d}t_k, & 0 \le t_i \le t_r : \text{loading} \\ \displaystyle\int_{t_r}^{0} f_L\Big(\varphi(t_k), \sigma\Big(\varphi(t_k)\Big)\Big) \times \varphi'(t_k)\mathrm{d}t_k + \int_{t_i}^{t_r} f_U\Big(\varphi(t_k), \sigma\Big(\varphi(t_k)\Big)\Big) \times \varphi'(t_k)\mathrm{d}t_k, & t_r \le t_i \le t_p : \text{unloading.} \end{cases} \quad (7)$$

Thus, the displacement time-history can be estimated using (7).

3. Closed-Form Solution

Using (7), closed-form solutions can be obtained for several simplified cases [28]. In this article, a closed-form approximation is developed for the following simplifications:

(a) Linearly decaying overpressure time-history with zero rise-time (Figure 3, (8)),

$$P(t_k) = P_o\left(1 - \frac{t_k}{t_{eq}}\right), \quad (8)$$

where P_o and t_{eq} are peak overpressure and equivalent positive phase duration, respectively. The reason behind choosing the special case with zero rise-time is the popularity of approximating the actual decay of the incidental pressure by an equivalent triangular pressure pulse among practicing engineers [8, 22]. It is to mention that design charts and empirical relations between the weapon yield, peak overpressure, and the equivalent positive phase durations are also available for equivalent triangular pulses with zero rise-time [5, 8, 29]. Thus, for practicing engineers, a linear decay model with zero rise-time is more useful.

(b) Bilinear hysteretic stress-strain model [8] with the loading secant modulus (M_L) and strain recovery ratio (r) as parameters (Figure 2).

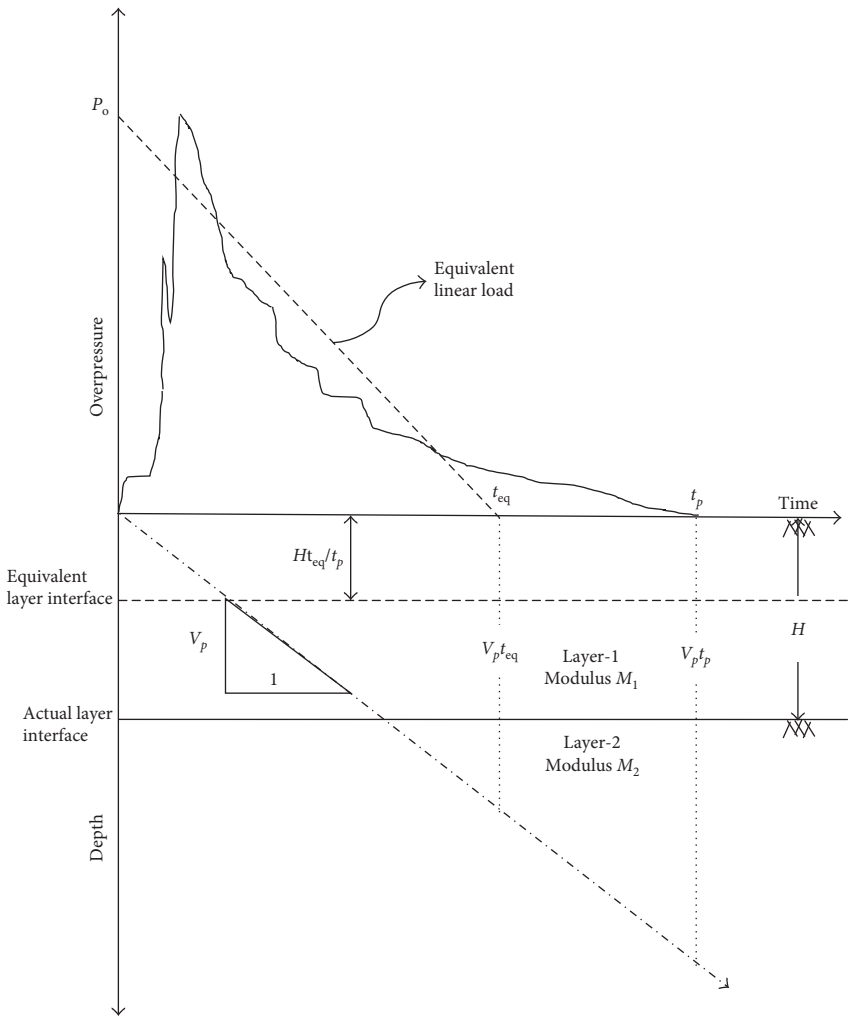

Figure 3: Scaling of equivalent ground media.

(c) Attenuation coefficient (α) is given by the following equation [8, 30]:

$$\alpha = \left(1 + \frac{z}{L_w}\right)^{-1}, \tag{9}$$

where $L_w = 0.971 \times W^{1/3} \times P_o^{-1/2} \times V_L$,

where W is the yield of the explosion in kiloton and V_L is the wave propagation velocity of the peak overpressure front.

(d) Using (4), f_{rz} is determined as 1 for the bilinear stress-strain model. However, due to nonlinear stress-strain behaviour, f_{rz} is usually greater than 1. Wilson and Sibley [17] and Batdorf [23] recommended a range of 1.5 to 2. Hereafter, f_{rz} is denoted as f and assumed to be constant with depth.

(e) A constant but representative P-wave velocity V_p of ground media is assumed.

Using assumptions (a)–(e), integral for loading fronts in (7) (with $t_r \to 0$) between general time instants t_x and t_{x+1} is written as $\mathrm{Lim}_{t_r \to 0}\left[\int_{t_x}^{t_{x+1}} f_L(\varphi(t_k), \sigma(\varphi(t_k))) \times \varphi'(t_k) \mathrm{d}t_k\right] = P_o / M_L \times \mathrm{Lim}_{t_r \to 0} L(t_x \to t_{x+1})$, where $L(t_x \to t_{x+1})$ can be shown to be given by the following equation:

$$L(t_x \longrightarrow t_{x+1}) = \frac{(f-1)t_i + t_r}{(f-1)L_w - t_r V_p} \times \left[\frac{L_w V_p}{(f-1)} \ln\left(\frac{(f-1)t_{x+1} + t_r}{(f-1)t_x + t_r}\right) + \frac{L_w\left(L_w + V_p t_i\right)}{\left(t_r + f t_i - t_i\right)}\right.$$
$$\left. \times \ln\left(\frac{\left(fL_w - L_w - t_r V_p\right)t_{x+1} + t_r\left(L_w + V_p t_i\right)}{\left(fL_w - L_w - t_r V_p\right)t_x + t_r\left(L_w + V_p t_i\right)} \times \frac{(f-1)t_x + t_r}{(f-1)t_{x+1} + t_r}\right)\right]. \tag{10}$$

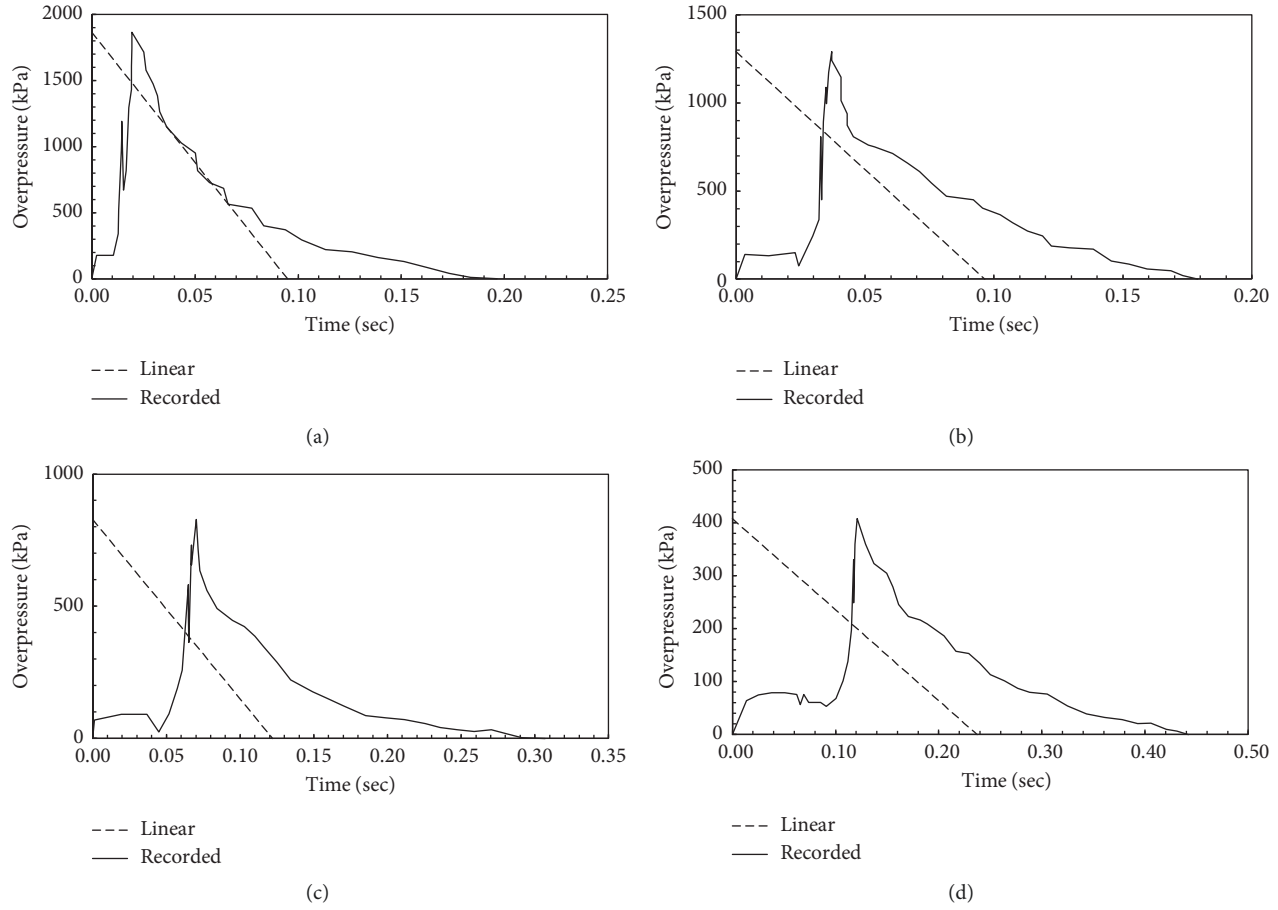

Figure 4: Measured and equivalent (linear) overpressure time-histories for shot Priscilla at stations (a) P1, (b) P2, (c) P3, and (d) P4 (measured overpressure time-histories [21]).

It is to clarify that the overpressure time-history defined by the piecewise function $P(t_k)$ such that $P(t_k) = P_o t_k / t_r$ for $t_k \le t_r$ and $P(t_k) = P_o(1 - (t_k - t_r))/(t_{eq} - t_r)$ for $t_r \le t_k \le t_{eq}$ converges to (8) in the limiting case when $t_r \to 0$. Therefore, the expression $L(t_x \to t_{x+1})$ in (10) is first obtained for a case of finite t_r and then it is evaluated for the case when $t_r \to 0$ to determine the solution for overpressure time-history of (8). Similarly, the integral for unloading fronts in (7) (with $t_r \to 0$) between general time instants t_x and t_{x+1} can be written as $\int_{t_{x+1}}^{t_x} f_U(\varphi(t_k), \sigma(\varphi(t_k))) \times \varphi'(t_k) \mathrm{d}t_k = (P_0/M_L) \times U(t_x \to t_{x+1})$, where $U(t_x \to t_{x+1})$ can be shown to be given by the following equation:

$$U(t_x \longrightarrow t_{x+1}) = L_w \left[1 - \frac{r f L_w}{t_p V_p} - \frac{r t_i}{t_p}\right] \ln\left(\frac{f L_w + V_p t_i - V_p t_x}{f L_w + V_p t_i - V_p t_{x+1}}\right) + \frac{r L_w (t_{x+1} - t_x)}{t_p}. \tag{11}$$

By setting the appropriate values of t_x and t_{x+1} in (10) and (11), the closed-form integrals between desired time instants can easily be evaluated. Thus, the closed-form solution is given by the following equation:

$$u_i = \frac{P_o}{M_L} \lim_{t_r \to 0} [L(0 \longrightarrow t_r) + U(t_r \longrightarrow t_i)]. \tag{12}$$

The closed-form solution is further extended to accommodate multiple ground layers. This requires the determination of time instants t_x and t_{x+1} during which the wave fronts pass through a particular layer. For illustration, a layered ground medium with an interface at depth H with the modulus of top layer as M_1 and modulus of bottom layer as M_2 is considered as shown in Figure 3. This leads to the three cases (Table 1) and corresponding displacement solutions (shown in Table 1).

4. Validation

The proposed closed-form solution is validated against the field data from an atmospheric nuclear test conducted at Frenchman Flat (Nevada). Perret [21] presented the measured overpressure time-histories (Figure 4) along with corresponding peak ground displacements at different distances from GZ (Table 2) for a 37 kt nuclear explosion at

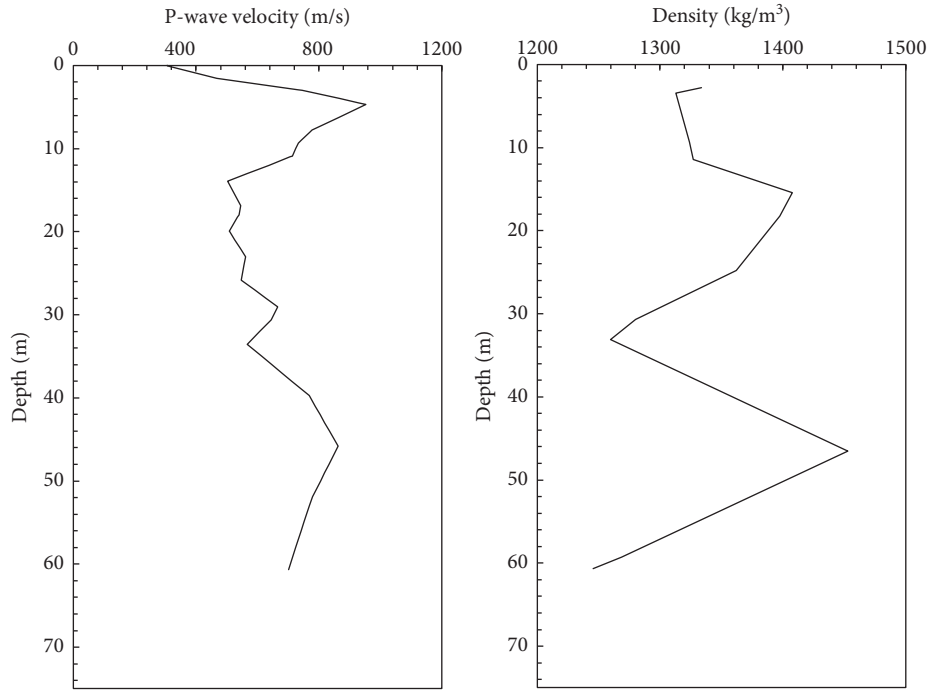

Figure 5: P-wave velocity and geomaterial density profile at Frenchman Flat, NTS [21].

a height of 214 m. Model input parameters for above mentioned nuclear test are determined as follows.

The recorded overpressure time-histories are converted to equivalent linearly decaying overpressure time-histories (Figure 4). Equivalent overpressure time-histories are given by (8) such that the peak overpressure (P_o) is equal to the recorded peak overpressure, and equivalent positive phase duration t_{eq} is given by the following equation:

$$t_{eq} = \frac{2I_p}{P_o}, \tag{13}$$

where I_p is the positive phase impulse (area under the recorded overpressure time-history). It is worth mentioning, though the rise-time is taken to be zero in the equivalent overpressure time-history in (8), that the effect of non-zero rising time has been accounted for by considering the total positive phase impulse (in (13)) which includes the area under the rising and decaying portions of actual overpressure time-history. Therefore, it is expected that setting the rise-time as zero in (8) would have a negligible impact on the magnitude of peak displacement. Furthermore, the ratios of length of rise-time to total positive phase duration for the four cases (P1, P2, P3, and P4) are 0.10, 0.21, 0.23, and 0.27, respectively. This indicates that rise-time is reasonably small near ground zero; however, the relative length of rise-time increases with increasing distance from ground zero. Thus, it is expected that the errors (if any) due to setting rise-time to zero would be more pronounced only at distances far away from ground zero. Even in such cases, a closed-form solution can be developed using (7) by setting a finite rise-time. However, it is worth noting that at far away distances (from ground zero), other important factors related to outrunning ground motion would start governing [31].

The initial pulse moving at seismic P-wave velocity (V_p) penetrates to a depth of $V_p t_{eq}$ for equivalent case, whereas for actual case, it penetrates to a depth of $V_p t_p$. It is noted that the depth of the stressed zone in the equivalent case is smaller compared to the actual case as equivalent duration (t_{eq}) is smaller than the actual positive phase duration (t_p) (Figure 4). Thus, all depth-dependent parameters are scaled by a factor SF = t_p/t_{eq}, such that the total depth of the stressed zone becomes SF × $V_p t_{eq} = V_p t_p$ with the depth of the top layer being H/SF, and with a characteristic attenuation length of L_w/SF. Based on the variation of P-wave velocity with depth at Frenchman Flat (Figure 5), the average P-wave velocity (V_p) is estimated as 658.69 m/s. Whitman [4] presented the representative constrained modulus for Frenchman Flat interpreted from different experimental techniques (Table 3). Whitman [4] also emphasized that all aspects of stress-strain behaviour of geomaterials under blast loading are not captured by a single test and advocated to choose the modulus judiciously. The stress attenuation coefficient is calculated using (9) with scaled L_w (Table 4). Using the closed-form solution (shown in Table 1), parametric variations are studied (Table 5) and peak displacements (Table 6) are estimated.

The parametric studies (Table 5) highlight that the proposed model is most sensitive to the constrained modulus compared to other parameters and choice of the modulus is also subjective for engineers. However, based on the parametric studies, the last column "Recommended Value" of Table 5 provides some guidelines to select the constrained modulus. With increasing

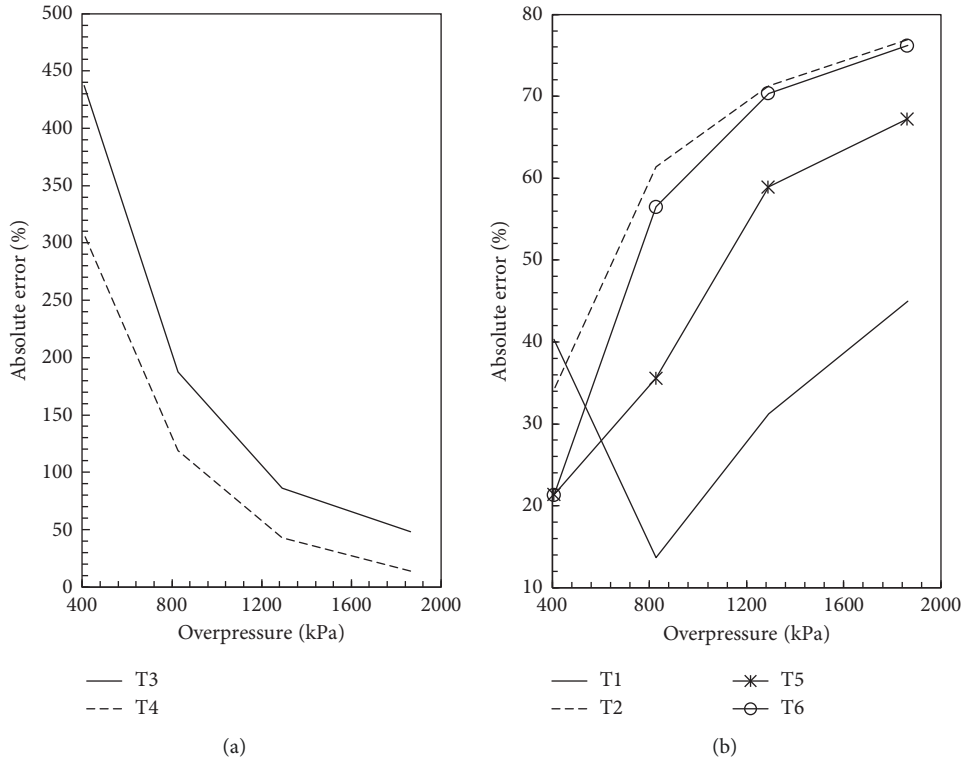

Figure 6: Variation of error in estimated peak displacement using constrained modulus determined from different experimental techniques: (a) T3 and T4 and (b) T1, T2, T5, and T6. T1: deduced from observed ground motion; T2: calculated from seismic velocity; T3: triaxial tests: initial loading; T4: dynamic 1-D compression test: initial loading; T5: triaxial tests: reloading; T6: resonant column test.

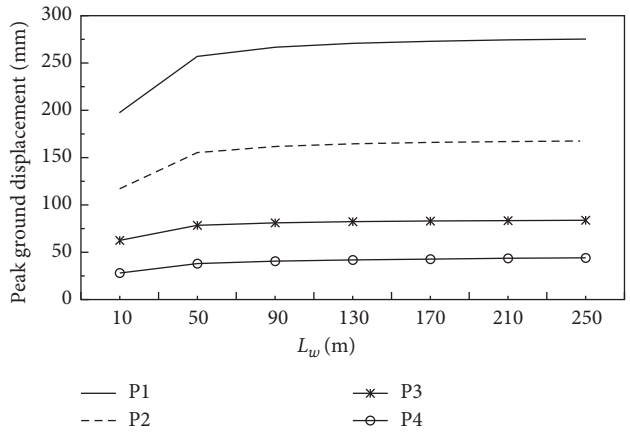

Figure 7: Variation of peak ground displacement with attenuation characteristic length L_w.

availability of similar case studies, these guidelines can further be refined.

5. Comparison with UFC Model

The UFC manual [22] provides an expression for air-blast-induced peak vertical displacement based on one-dimensional elastic wave propagation:

$$u_i\big|_{\max} = \frac{I_p}{\rho V_p}, \tag{14}$$

where ρ is the bulk density of geomaterials. To estimate peak displacements using (14), positive phase impulse (I_p) is taken from Table 2. Representative P-wave velocity (V_p) and density (ρ) are taken as 658.69 m/s and 1331 kg/m^3, respectively, taking into account the variation with depth (Figure 5). Computed peak displacements using the proposed model and UFC model are shown in Figure 9 along with the measured field values. It can be clearly seen that the predicted values of the proposed model are in good agreement with the measured values and the UFC model significantly underestimates the peak displacements under high overpressures (with increasing war head capacity).

6. Conclusions

A closed-form expression is developed to estimate nuclear-air-blast-induced free-field ground displacement that takes into account peak overpressure, positive phase impulse, depth of layer interface, representative constrained modulus of each layer, strain recovery, stress attenuation, P-wave velocity, and velocity ratio. The solution is validated against a nuclear test conducted at Frenchman Flat (Nevada) and the following conclusions are arrived at:

(i) Peak ground displacement estimates are quite sensitive to the constrained modulus, and a judicious

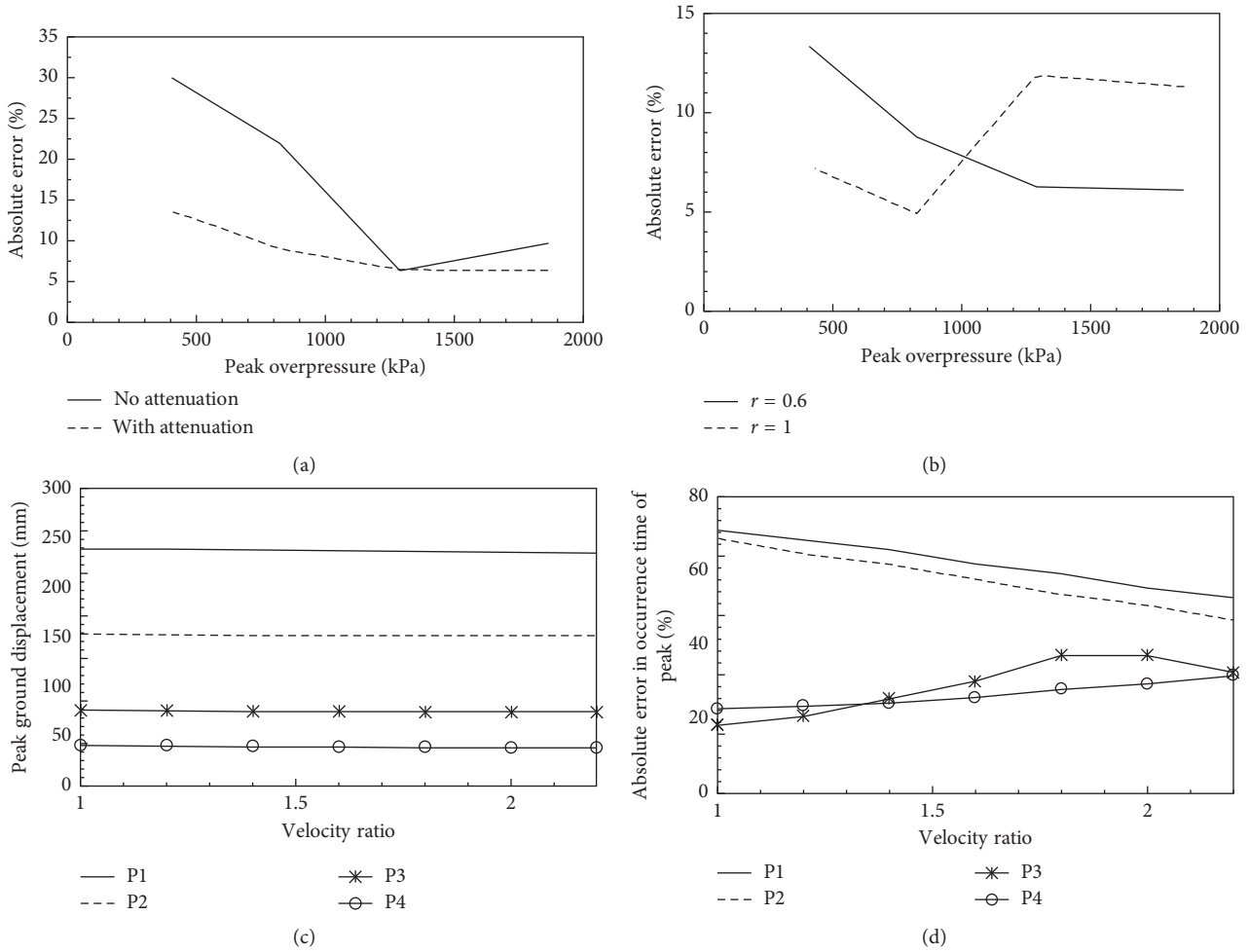

Figure 8: Effect of (a) attenuation; (b) strain recovery ratio; (c) velocity ratio on estimated ground displacement; (d) velocity ratio on time of occurrence of peak displacement.

selection of appropriate constrained modulus based on the magnitude of applied overpressure is recommended.

(ii) Based on the presented case study, two guidelines are recommended to select the appropriate modulus: (a) shallow ground layers are likely to have modulus values determined by unconfined or triaxial compression test and deep ground layers are likely to have modulus values computed from seismic velocity test, and (b) constrained modulus increases with decreasing ratio of applied stress to overburden.

(iii) Effect of attenuation should be accounted for low overpressures and may be neglected at higher overpressures (or high war head capacities).

(iv) The velocity ratio affects mainly the time of occurrence of peak ground displacement and not the

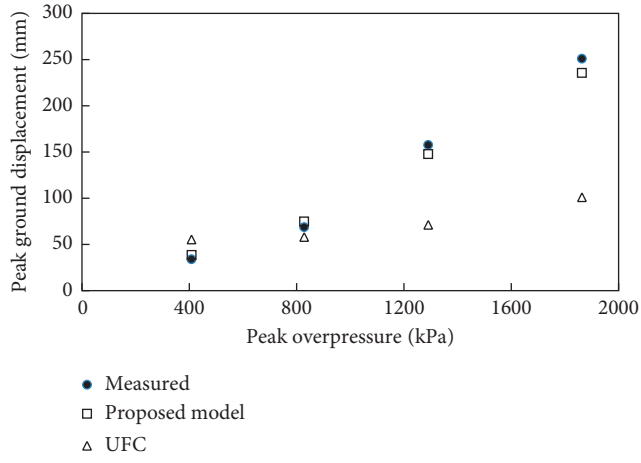

Figure 9: Comparison between measured and estimated peak ground displacements.

Table 1: Displacement solutions for the double-layered media.

Case	Explanation	Displacement equation
1	When all loading and unloading fronts are in layer-1 ($t_i \le H/V_p$).	$u_i = P_o \lim_{t_r \to 0} \left[\frac{L(0 \to t_r)}{M_1} + \frac{U(t_r \to t_i)}{M_1} \right]$
2	When some loading fronts have crossed layer-1 and remaining loading fronts along with all unloading fronts are in layer-1 ($H/V_p < t_i \le fH/V_p$). Here, the first task is to determine those loading fronts which have crossed layer-1. This can be obtained by equating loading front velocity multiplied with travel time with the depth of layer. The loading front velocity of the kth front can be written using (3) as $V_p/\{(f-1)(t_k/t_r)+1\}$, and travel time is $(t_i - t_k)$. Thus, the last loading front to reach at depth H by the time t_i would be given by $t_{kH} = t_r(V_p t_i - H)/\{H(f-1) + V_p t_r\}$.	$u_i = P_o \lim_{t_r \to 0} \left[\frac{L(0 \to t_{kH})}{M_2} + \frac{L(t_{kH} \to t_r)}{M_1} + \frac{U(t_r \to t_i)}{M_1} \right]$
3	When all loading fronts are in layer-2 and some unloading fronts have crossed layer-1 ($fH/V_p < t_i$). Similar to case 2, the last unloading front to reach at depth H by the time t_i would be given by $t_{kH} = t_i - fH/V_p$.	$u_i = P_o \lim_{t_r \to 0} \left[\frac{L(0 \to t_r)}{M_2} + \frac{U(t_r \to t_i - fH/V_p)}{M_2} + \frac{U(t_i - fH/V_p \to t_i)}{M_1} \right]$

Table 2: Details of recording stations.

Station designation	Range (m)	Peak overpressure (kPa)	Positive phase duration (sec)	Positive phase impulse (kPa-sec)	Equivalent duration (sec)	Scale factor (SF)
P1	198	1863	0.196	88.32	0.0948	2.07
P2	259	1290	0.179	62.18	0.0964	1.86
P3	320	828	0.307	50.54	0.1221	2.51
P4	411	408	0.442	48.34	0.2371	1.86

Table 3: Constrained modulus of playa silt at Frenchman Flat [4].

Method	Notation	Constrained modulus (MPa)	
		For depths less than 18 m	For depths more than 18 m
Deduced from observed ground motion	T1	96.6	552
Calculated from seismic velocity	T2	242	1035
Triaxial tests: initial loading	T3	55.2	103.5
Dynamic 1-D compression test: initial loading	T4	69	138
Triaxial tests: reloading	T5	276	448.5
Resonant column test	T6	276	759

Table 4: Scaling of attenuation characteristic length (L_w).

Station designation	W (kt)	P_o (kPa)	V_p (m/s)	L_w (m)	Scaled L_w (m)
P1	37	1863	658.69	48.58	23.47
P2		1290	658.69	58.38	31.44
P3		828	658.69	72.88	28.98
P4		408	658.69	103.84	55.70

magnitude under higher overpressures. Therefore, the velocity ratio becomes important when design calculations utilize the complete displacement time-history such as in case of shock spectra.

(v) A complete strain recovery is a better representation of actual conditions under low overpressure zones, and under higher overpressures, a partial strain recovery is recommended.

Table 5: Parametric studies carried out on the proposed closed-form solution.

Parameter	Parametric study	Observation	Recommended value
M_1 and M_2	Parameters M_1 and M_2 based on six different methods are adopted from Table 3.	Peak ground displacements are very sensitive to the constrained modulus value.	Observed results are consistent with the observations of Wilson and Sibley [17].
	Other parameters kept constant at $r = 0.6$; $f = 2$; L_w adopted from Table 4.	Average coefficient of variation in peak displacement estimates = 83%.	(1) Shallow ground layers are likely to have modulus values determined by unconfined or triaxial compression test, and deep ground layers are likely to have modulus values computed from seismic velocity test or resonant column test. The justification to this variation in selection of modulus values can be attributed to the small strains associated with deeper layers and higher strains at shallow depths.
	Variation of absolute percentage errors in estimated peak ground displacements is plotted against peak overpressures in Figures 6(a) and 6(b).	Estimates are close to measured values if higher modulus values are used for smaller overpressures.	(2) Constrained modulus increases with decreasing ratio of applied stress to overburden. For higher overpressures, the overstress ratio would be higher and therefore modulus value will be lower compared to lower overpressures. An optimal choice of constrained modulus values is adopted as shown in Table 6. The computed displacements are found to be in good agreement with measured displacements (Table 6).
L_w	L_w is varied from 10 m to 250 m. Other parameters kept fixed at M_1 and M_2 adopted from Table 6; $f = 2$; $r = 0.6$.	As L_w increases (or α decreases), peak displacement increases.	Attenuation has to be taken into account under low overpressures, and it can be ignored under high overpressures.
	Estimated peak displacements are plotted against L_w as shown in Figure 7. Errors in estimated peak displacements for the attenuating medium and non-attenuating medium are also plotted against peak overpressure in Figure 8(a).	Beyond L_w of 250 m, the peak ground displacement does not increase, and $L_w \geq 250$ is considered as the non-attenuating medium.	
r	Two cases are considered: (i) full strain recovery $r = 1$ and (ii) partial strain recovery $r = 0.6$.		Under low overpressure, ground is not stressed beyond its elastic limit, and hence full strain recovery is a better representation of actual conditions in low overpressure zones.
	Other parameters fixed at M_1 and M_2 adopted from Table 6; $f = 2$; L_w adopted from Table 4.	Assumption of full strain recovery gives less errors as compared to partial strain recovery under low overpressures.	A lower strain recovery causes higher permanent deformations and increases peak ground displacement compared to elastic case (i.e., unit strain recovery ratio). Under higher overpressures, the ground is stressed beyond its elastic limit and the assumption of partial strain recovery is recommended.
	Errors in estimated peak displacement for the two cases are plotted as shown in Figure 8(b).		
f	f is varied from 1.0 to 2.2.	Under high overpressure (P1 and P2), error in occurrence time of peak displacement reduces significantly with increasing f.	f has insignificant effect on magnitude of estimated peak displacements. However, as the velocity ratio increases, the rise-time of overstress pulse with depth also increases and affects the occurrence time of the peak displacement.
	Other parameters fixed at M_1 and M_2 adopted from Table 6; $r = 0.6$; L_w adopted from Table 4. Estimated peak displacements are plotted against f (Figure 8(c)). Error in occurrence time of peak displacement are also plotted against f (Figure 8(d)).	Error increases marginally under lower overpressures as the velocity ratio is close to 1 under lower stress (in (3) when $t_k \to 0$).	

Table 6: Suggested combination of modulus values and corresponding estimated peak displacements.

Station designation	M_1 (MPa) (depths less than 18 m)	M_2 (MPa) (depths more than 18 m)	Estimated peak displacement (mm)	Experimental records (mm)	% error
P1	55.2 triaxial tests: initial loading	552 deduced from observed ground motion	235.59	250.95	6.12
P2	69 dynamic 1-D compression test: initial loading	759 resonant column test	147.68	157.56	6.27
P3	69 dynamic 1-D compression test: initial loading	759 resonant column test	74.79	68.75	8.79
P4	96.6 deduced from observed ground motion	1035 calculated from seismic velocity	38.49	33.95	13.37

(vi) The proposed model closely estimates the experimental values at all overpressures, whereas the UFC model significantly underestimates the peak ground displacements at high overpressures.

Notations

$\alpha(Z_{ki})$: Attenuation coefficient at depth Z_{ki}
ε_{iz}: Strain at time t_i at depth "z"
ε_{pz}: Peak strain level in geomaterial at depth "z"
ε_{rz}: Residual strain level in geomaterial at depth "z"
f: Representative velocity ratio (between P-wave velocity and peak stress velocity) of ground media
f_{kz}: Ratio of P-wave velocity to wave velocity corresponding to the kth overpressure front at depth "z"
f_L: Functional form for the loading branch of the stress-strain curve
f_{rz}: Ratio of P-wave velocity to wave velocity corresponding to the peak overpressure front at depth "z"
f_U: Functional form for the unloading branch of the stress-strain curve
H: Depth of the top ground layer
I_p: Positive phase impulse of overpressure time-history
L_w: Characteristic attenuation length
M_L: Loading secant modulus
M_2: Modulus of bottom layer
M_1: Modulus of top layer
P_o: Peak overpressure
$P(t_k)$: Pressure magnitude of the kth overpressure front
r: Strain recovery ratio
ρ: Bulk-density of geomaterials
SF: Scale factor
σ_{pz}: Peak stress level in geomaterial at depth "z"
t_{eq}: Equivalent positive phase duration of linearly decaying overpressure time-history
t_k: Time when the kth overpressure front arrives at the point of interest on ground surface
t_{kH}: Time of arrival of the last loading front to reach at depth H (by the time t_i)
t_p: Positive phase duration of overpressure time-history
t_r: Rise-time to peak overpressure in overpressure time-history
u_i: Vertical ground displacement at time t_i
V_p: Representative P-wave velocity of ground media
V_L: Representative wave propagation velocity of the peak overpressure front in ground
V_{kz}: Wave velocity of the kth stress front at depth "z"
W: Yield of the explosion
Z_{ki}: Depth penetrated by the kth overpressure front at time t_i
σ_{iz}: Stress at time t_i at depth "z"
Z_{0i}: Depth penetrated by initial pulse at time t_i
Z_{pi}: Depth penetrated by the peak overpressure front at time t_i
$(\partial\sigma_z/\partial\varepsilon_z)|_{\sigma=0}$: Tangential modulus at initial stress level at depth "z"
$(\partial\sigma_z/\partial\varepsilon_z)|_{\sigma_{rz}}$: Tangential modulus at peak stress level at depth "z."

Conflicts of Interest

The authors declare that there are no conflicts of interest regarding the publication of this paper.

References

[1] S. Pinto, "Underground construction of nuclear power reactors," *Nuclear Engineering and Design*, vol. 61, no. 3, pp. 441–458, 1980.
[2] C. V. Chester and G. P. Zimmerman, "Civil defense shelters: a state-of-the-art assessment," *Tunnelling and Underground Space Technology*, vol. 2, no. 4, pp. 401–428, 1987.
[3] S. Glasstone and P. J. Dolan, *The Effects of Nuclear Weapons*, Castle House Publications, London, UK, 1980.
[4] R. V. Whitman, *The Response of Soils to Dynamic Loadings; Report 26, Final Report*, Massachusetts Institute of Technology, Cambridge, MA, USA, 1970.

[5] R. E. Crawford, C. J. Higgins, and E. H. Bultmann, *The Air Force Manual for Design and Analysis of Hardened Structures, Final Report Jun 71-May 74 (No. AD-B-004152/5)*, Civil Nuclear Systems Corporation, Albuquerque, NM, USA, 1974.

[6] B. M. Das, *Fundamentals of Soil-Dynamics*, Chapter 4, Elsevier, Amsterdam, Netherlands, 1983.

[7] H. L. Brode, *A Review of Nuclear Explosion Phenomena Pertinent to Protective Construction, R 425 PR*, The Rand Corporation, Santa Monica, CA, USA, 1964.

[8] M. S. Agbabian, *Design of Structures to Resist Nuclear Weapon Effects, ASCE Manual on Engineering Practice*, Vol. 42, ASCE, Reston, VA, USA, 1985.

[9] J. H. Prevost, *DYNAFLOW: A Nonlinear Transient Finite Element Analysis Program*, Princeton University, Princeton, NJ, USA, 1981.

[10] F. Rischbieter and K. Michelmann, *Bodenwelle bei Gasexplosionen. Beitrag der induzierten Bodenwelle zur Belastung von KKW-Strukturen*, Batelle-Institut, Frankfurt, Germany, 1984.

[11] K. J. Kim and S. E. Blouin, *Response of Saturated Porous Nonlinear Materials to Dynamic Loadings*, Applied Research Associates Inc., South Royalton, VT, USA, 1984.

[12] H. Werkle and G. Waas, "Analysis of ground motion caused by propagating air pressure waves," *Soil Dynamics and Earthquake Engineering*, vol. 6, no. 4, pp. 194–202, 1987.

[13] Z. Yang, "Finite element simulation of response of buried shelters to blast loadings," *Finite Elements in Analysis and Design*, vol. 24, no. 3, pp. 113–132, 1997.

[14] Z. Wang, H. Hao, and Y. Lu, "A three-phase soil model for simulating stress wave propagation due to blast loading," *International Journal for Numerical and Analytical Methods in Geomechanics*, vol. 28, no. 1, pp. 33–56, 2004.

[15] Y. Lu and Z. Wang, "Characterization of structural effects from above-ground explosion using coupled numerical simulation," *Computers & Structures*, vol. 84, no. 28, pp. 1729–1742, 2006.

[16] T. Bierer and C. Bode, "A semi-analytical model in time domain for moving loads," *Soil Dynamics and Earthquake Engineering*, vol. 27, no. 12, pp. 1073–1081, 2007.

[17] S. D. Wilson and E. A. Sibley, "Ground displacements from air-blast loading," *Journal of the Soil Mechanics and Foundations Division*, vol. 88, no. 6, pp. 1–32, 1962.

[18] M. L. Baron, I. Nelson, and I. Sandler, *Investigation of Air Induced Ground Shock Effect Resulting from Various Explosive Sources. Report 2, Influence of Constitutive Models on Ground Motion Predictions*, Weidlinger Associates, New York, NY, USA, 1971.

[19] Z. Wang and Y. Lu, "Numerical analysis on dynamic deformation mechanism of soils under blast loading," *Soil Dynamics and Earthquake Engineering*, vol. 23, no. 8, pp. 705–714, 2003.

[20] S. Wang, L. Shen, F. Maggi, A. El-Zein, and G. D. Nguyen, "Uniaxial compressive behavior of partially saturated granular media under high strain rates," *International Journal of Impact Engineering*, vol. 102, pp. 156–168, 2017.

[21] W. R. Perret, *Ground Motion Studies at High Incident Overpressure*, Sandia Corporation, Albuquerque, NM, USA, 1960.

[22] UFC Manual, *Structures to Resist the Effects of Accidental Explosions*, US DoD, Washington, DC, USA, UFC 3-340-02, 2008.

[23] S. B. Batdorf, "Air-inducedground shock: a one-dimensional theory," in *Proceedings of International Symposium on Wave Propagation and Dynamic Properties of Earth Materials, Albuquerque, NM, USA, August 1967*, G. Triandafilidis, Ed., pp. 423–432, Aerospace Corp., San Bernardino, CA, USA, 1969.

[24] S. L. Kramer, *Geotechnical Earthquake Engineering*, Pearson Education, Delhi, India, 1996.

[25] X. Tong and C. Tuan, "Viscoplastic cap model for soils under high strain rate loading," *Journal of Geotechnical and Geoenvironmental Engineering*, vol. 2, no. 206, pp. 206–214, 2007.

[26] J. An, C. Y. Tuan, B. A. Cheeseman, and G. A. Gazonas, "Simulation of soil behavior under blast loading," *International Journal of Geomechanics*, vol. 11, no. 4, pp. 323–334, 2011.

[27] P. Y. Hicher and J. F. Shao, *Constitutive Modeling of Soils and Rocks*, John Wiley & Sons, Hoboken, NJ, USA, 2013.

[28] S. Pathak and G. V. Ramana, "Air-blast induced ground displacement," *Procedia Engineering*, vol. 173, pp. 555–562, 2017.

[29] N. M. Newmark and J. D. Haltiwanger, *Air Force Design Manual, Principles and Practices for Design of Hardened Structures*, University of Illinois at Urbana–Champaign, Champaign, IL, USA, 1962.

[30] A. J. Hendron Jr. and H. E. Auld, "Effectof soil properties on the attenuation of airblastnduced ground motions," in *Proceedings of International Symposium on Wave Propagation and Dynamic Properties of Earth Materials, Albuquerque, NM, USA, August 1967*, G. Triandafilidis, Ed., pp. 29–47, University of Illinois, Urbana, IL, USA, 1969.

[31] I. Nelson and G. Y. Baladi, "Outrunning ground shock computed with different models," *Journal of the Engineering Mechanics Division*, vol. 103, no. 3, pp. 377–393, 1977.